UNIVERSITY OF AMSTERDAM

UvA-DARE (Digital Academic Repository)

The balance between $G\alpha_i$-Cdc42/Rac and $G\alpha_{12/13}$-RhoA pathways determines endothelial barrier regulation by sphingosine-1-phosphate

Reinhard, N.R.; Mastop, M.; Yin, T.; Wu, Y.; Bosma, E.K.; Gadella, T.W.J.; Goedhart, J.; Hordijk, P.L.

DOI
10.1091/mbc.E17-03-0136

Publication date
2017

Document Version
Final published version

Published in
Molecular Biology of the Cell

License
CC BY-NC-SA

Link to publication

Citation for published version (APA):
Reinhard, N. R., Mastop, M., Yin, T., Wu, Y., Bosma, E. K., Gadella, T. W. J., Goedhart, J., & Hordijk, P. L. (2017). The balance between $G\alpha_i$-Cdc42/Rac and $G\alpha_{12/13}$-RhoA pathways determines endothelial barrier regulation by sphingosine-1-phosphate. *Molecular Biology of the Cell*, *28*(23), 3371-3382. https://doi.org/10.1091/mbc.E17-03-0136

General rights
It is not permitted to download or to forward/distribute the text or part of it without the consent of the author(s) and/or copyright holder(s), other than for strictly personal, individual use, unless the work is under an open content license (like Creative Commons).

Disclaimer/Complaints regulations
If you believe that digital publication of certain material infringes any of your rights or (privacy) interests, please let the Library know, stating your reasons. In case of a legitimate complaint, the Library will make the material inaccessible and/or remove it from the website. Please Ask the Library: https://uba.uva.nl/en/contact, or a letter to: Library of the University of Amsterdam, Secretariat, P.O. Box 19185, 1000 GD Amsterdam, The Netherlands. You will be contacted as soon as possible.
UvA-DARE is a service provided by the library of the University of Amsterdam (https://dare.uva.nl)

Download date:12 Oct 2026

The balance between $G\alpha_i$-Cdc42/Rac and $G\alpha_{12/13}$-RhoA pathways determines endothelial barrier regulation by sphingosine-1-phosphate

Nathalie R. Reinhard[a,b,c], Marieke Mastop[a], Taofei Yin[d], Yi Wu[d], Esmeralda K. Bosma[a], Theodorus W. J. Gadella Jr.[a], Joachim Goedhart[a,†,*], and Peter L. Hordijk[a,b,c,e,†,*]

[a]van Leeuwenhoek Centre for Advanced Microscopy, Molecular Cytology, Swammerdam Institute for Life Sciences, University of Amsterdam, 1098 XH Amsterdam, Netherlands; [b]Molecular Cell Biology and [c]University of Amsterdam Academic Medical Centre–Landsteiner Laboratory, Sanquin Research, 1066 CX Amsterdam, Netherlands; [d]Center for Cell Analysis and Modeling, University of Connecticut Health Center, Farmington, CT 06030; [e]Department of Physiology, Free University Medical Center, 1081 HZ Amsterdam, Netherlands

ABSTRACT **The bioactive sphingosine-1-phosphatephosphate (S1P) is present in plasma, bound to carrier proteins, and involved in many physiological processes, including angiogenesis, inflammatory responses, and vascular stabilization. S1P can bind to several G-protein–coupled receptors (GPCRs) activating a number of different signaling networks. At present, the dynamics and relative importance of signaling events activated immediately downstream of GPCR activation are unclear. To examine these, we used a set of fluorescence resonance energy transfer–based biosensors for different RhoGTPases (Rac1, RhoA/B/C, and Cdc42) as well as for heterotrimeric G-proteins in a series of live-cell imaging experiments in primary human endothelial cells. These experiments were accompanied by biochemical GTPase activity assays and transendothelial resistance measurements. We show that S1P promotes cell spreading and endothelial barrier function through $S1PR_1$-$G\alpha_i$-Rac1 and $S1PR_1$-$G\alpha_i$-Cdc42 pathways. In parallel, a $S1PR_2$-$G\alpha_{12/13}$-RhoA pathway is activated that can induce cell contraction and loss of barrier function, but only if $G\alpha_i$-mediated signaling is suppressed. Our results suggest that $G\alpha_q$ activity is not involved in S1P-mediated regulation of barrier integrity. Moreover, we show that early activation of RhoA by S1P inactivates Rac1 but not Cdc42, and vice versa. Together, our data show that the rapid S1P-induced increase in endothelial integrity is mediated by a $S1PR_1$-$G\alpha_i$-Cdc42 pathway.**

Monitoring Editor
Peter Van Haastert
University of Groningen

Received: Mar 3, 2017
Revised: Sep 14, 2017
Accepted: Sep 19, 2017

INTRODUCTION

Endothelial cells (ECs) line blood and lymphatic vessels, forming a semipermeable barrier between the blood and underlying tissue (Aird, 2007a,b). By sensing environmental changes, this cell layer regulates the transport of oxygen and essential nutrients to all organ systems in the human body (Pappenheimer *et al.*, 1951; Del Vecchio *et al.*, 1987; Siflinger-Birnboim *et al.*, 1987). These continuous sensing capabilities are required to maintain vascular homeostasis and form the basis of many physiological and disease-related processes.

This article was published online ahead of print in MBoC in Press (http://www.molbiolcell.org/cgi/doi/10.1091/mbc.E17-03-0136) on September 27, 2017.

†These authors contributed equally to this work.

The authors declare no competing or financial interests.

Author contributions: N.R.R., M.M., and E.K.B. performed experiments. N.R.R. analyzed the data and wrote the manuscript. Y.W. and T.Y. designed and constructed the DORA-Rho GTPase biosensors. T.W.J.G., J.G., and P.L.H. assisted with the experimental design and data interpretation. All authors approved the final manuscript.

*Address correspondence to: Peter L. Hordijk (p.hordijk@vumc.nl) or Joachim Goedhart (j.goedhart@uva.nl).

Abbreviations used: AJ, adherens junction; BSA, bovine serum albumin; CFP, cyan fluorescent protein; CRIB, Cdc42/Rac interactive binding; EC, endothelial cell; ECIS, Electrical Cell-substrate Impedance Sensing; FA, focal adhesion; FN, fibronectin; FRET, fluorescence resonance energy transfer; GAP, GTPase activating protein; GEF, guanine exchange factor; GPCR, G-protein–coupled receptor; HUVEC, human umbilical vein endothelial cell; mAb, monoclonal antibody; mTq2, mTurquoise2; NA, numerical aperture; pAb, polyclonal antibody; PBS, phosphate-buffered saline; PM, plasma membrane; PTX, pertussis toxin; RBD, Rho binding domain; RGS, regulator of G-protein signaling; RhoGEF, Rho guanine exchange factor; S1P, sphingosine-1-phosphate; TEM, transendothelial migration; TJ, tight junction; VE-cadherin, vascular endothelial cadherin protein.

© 2017 Reinhard *et al.* This article is distributed by The American Society for Cell Biology under license from the author(s). Two months after publication it is available to the public under an Attribution–Noncommercial–Share Alike 3.0 Unported Creative Commons License (http://creativecommons.org/licenses/by-nc-sa/3.0).

"ASCB®," "The American Society for Cell Biology®," and "Molecular Biology of the Cell®" are registered trademarks of The American Society for Cell Biology.

Supplemental Material can be found at:
http://www.molbiolcell.org/content/suppl/2017/09/25/mbc.E17-03-0136v1.DC1

Active participation of ECs in homeostasis is required not only to control the transport and diffusion of essential solutes, but also to carefully regulate many physiological processes, including inflammation, the constitutive and induced transendothelial migration (TEM) of immune cells, thrombosis, angiogenesis, and arteriogenesis (Nourshargh *et al.*, 2010; Korn and Augustin, 2015; Schaefer and Hordijk, 2015; van Hinsbergh *et al.*, 2015).

The endothelium-dependent functions and characteristics thus play a central role in vascular stabilization, a process that depends in particular on intercellular contacts between adjacent ECs. Endothelial intercellular contacts are mediated by two types of junctional complexes: adherens junctions (AJs) and tight junctions (TJs). Whereas TJs regulate the diffusion of water, ions, and small molecules, the AJs control more diverse and complex functions in the endothelium, such as limiting edema, matrix exposure, and leukocyte TEM, by translating extracellular force into intracellular signaling and regulating the cross-talk between cell–cell and cell–matrix adhesions (Mehta and Malik, 2006; Dejana *et al.*, 2008). AJs are mainly composed of the vascular endothelial cadherin protein (VE-cadherin), which is strictly required to establish EC–cell contacts and anchors AJs to the actin cytoskeleton via several adapter proteins (Lampugnani, 1995; Dejana, 1996; Giannotta *et al.*, 2013). Because signaling toward the actin cytoskeleton dynamically controls the loss and gain in barrier function, VE-cadherin plays a major role in junctional stability and thereby vascular integrity.

There are a large number of receptor agonists, including growth factors, hormones, and bioactive lipids, that regulate endothelial barrier function in positive or negative ways (Mehta and Malik, 2006). An important signaling molecule that, in most vessels, promotes VE-cadherin stabilization is sphingosine-1-phosphate (S1P; Lee *et al.*, 1999). This bioactive sphingolipid, produced by ECs, erythrocytes, and, to some extent, activated platelets (Yatomi *et al.*, 1997a; Yang *et al.*, 1999; Ancellin *et al.*, 2002; Kobayashi *et al.*, 2006; Hänel *et al.*, 2007; Ito *et al.*, 2007), is present in relatively high concentrations (100–600 nM) in plasma (Yatomi *et al.*, 1997a,b; Caligan *et al.*, 2000; Berdyshev *et al.*, 2005). Extracellular S1P can bind to five different G-protein–coupled receptors (GPCRs), termed $S1PR_{1–5}$, three of which ($S1PR_1$, $S1PR_2$, and $S1PR_3$) are expressed in ECs. Resting, healthy ECs express mainly the $S1PR_1$ and, to a lesser extent, the $S1PR_2$ and $S1PR_3$ as well (Fernández-Pisonero *et al.*, 2012). Activation of the $S1PR_1$ induces vascular stabilization and enhanced barrier function, while both the $S1PR_2$ and $S1PR_3$ have been linked to disruption of the endothelium (reviewed in Xiong and Hla [2014]). The balance in receptor subtype expression as well as plasma S1P concentration levels determines vascular integrity. Aberrant S1P plasma levels have been linked to multiple types of cancer, since binding to S1P receptors can promote tumor growth, angiogenesis, and metastasis (Pyne and Pyne, 2010). In addition, a shift in balance from dominant $S1PR_1$ to $S1PR_2$ signaling induces vascular permeability and inflammation (Sanchez *et al.*, 2007; Zhang *et al.*, 2013).

As described above, the output of S1P-mediated endothelial barrier regulation is already determined at the level of the receptors. These receptors couple to heterotrimeric G-proteins, which reside at the intracellular side of the plasma membrane (PM) and consist of a Gα subunit and a Gβγ-dimer. In S1P-mediated barrier regulation, it is believed that three different Gα subunits are involved; $G\alpha_i$, $G\alpha_{12/13}$, and $G\alpha_q$ (Poti *et al.*, 2014). The $S1PR_1$ is exclusively coupled to $G\alpha_i$, and inhibition of this G-protein prevents increased barrier function of endothelial monolayers (Garcia *et al.*, 2001; Liu *et al.*, 2001). The $S1PR_2$ and $S1PR_3$ couple to all three G-proteins, but how this receptor–G-protein coupling affects endothelial barrier regulation remains unexplored.

Downstream of heterotrimeric G-proteins, Rho guanine exchange factors (RhoGEFs) act to activate RhoGTPases, molecular switches that regulate cell morphology, polarity, adhesion, and migration through their differential control of F-actin dynamics (Jaffe and Hall, 2005; Ridley, 2006). The RhoGTPases Rac1, Cdc42, and RhoA are the most well-studied ones, with Rac1 stimulating actin polymerization and lamellipodia-driven migration, Cdc42 promoting filopodia formation, and RhoA stimulating F-actin stress fiber formation and cell contraction while counteracting Rac1-induced cell spreading (Ridley, 2015). By having strong effects on cell morphology and cytoskeletal dynamics, RhoGTPases are key regulators of endothelial barrier function. The contribution of Rac1, Cdc42, and RhoA in S1P-mediated barrier regulation was studied previously using biochemical approaches (Vouret-Craviari *et al.*, 2002; Breslin *et al.*, 2015), providing evidence that all three are activated by S1P.

Because biochemical approaches 1) have only limited temporal resolution, 2) have no spatial resolution, and 3) are difficult to quantify, we analyzed S1P-induced signaling in detail using fluorescence resonance energy transfer (FRET) biosensors for RhoGTPases and for heterotrimeric G-proteins in monolayers of primary human ECs. We show direct, rapid S1P-mediated $G\alpha_i$ and $G\alpha_{12/13}$ activation, while $G\alpha_q$ activation was lacking. In addition, FRET sensor measurements showed a sequential activation of Cdc42, RhoA, and Rac1 during S1P-mediated regulation of endothelial barrier function. The single-cell imaging approach reveals a detailed picture of signaling events in relation to cell morphology. Together, our results point to a model in which the balance between two opposing pathways determines EC morphology and monolayer integrity.

RESULTS

S1P promotes endothelial barrier function

Previous studies on S1P-mediated signaling in ECs have shown that extracellular S1P promotes vascular stabilization and increased barrier function (Lee *et al.*, 1999; Garcia *et al.*, 2001). To understand this barrier-promoting effect in more detail, different approaches were used to examine S1P effects at the cellular level. First, S1P stimulation of semiconfluent human umbilical vein EC (HUVEC) cells was combined with immunofluorescence analysis. This allowed detection of morphological changes, which are difficult to detect in confluent endothelial monolayers. Unstimulated ECs showed mixed phenotypes in terms of F-actin distribution as reflected by contractile (stress fiber) and protruding (cortical actin-based) regions within a single cell (Figure 1A). The cortical region of the cells showed enhanced phospho-paxillin levels, marking cortical focal adhesions (FAs), which correlated with cell spreading (Schaller and Parsons, 1995; Panetti, 2002). After 2 min of S1P stimulation, ECs showed an extensive increase in cortical actin, together with more pronounced phospho-paxillin at focal contacts and FAs in the periphery of the cell. After 30 min of S1P stimulation, this cortical actin–phospho-paxillin region disappeared and phospho-paxillin was detected in more centrally distributed FAs (Figure 1A).

In addition to the immunolabeling approach, we quantitatively analyzed the barrier-promoting effect of S1P using Electrical Cell-substrate Impedance Sensing (ECIS). S1P induced a fast increase in transendothelial electrical resistance of 20% (Figure 1B). In addition, after ectopic expression of mTurquoise2 (mTq2, a CFP), we measured morphological changes of single cells in an endothelial monolayer to provide an outline of the cell area. Measuring the temporal changes in the cell area of single mTq2-expressing ECs in

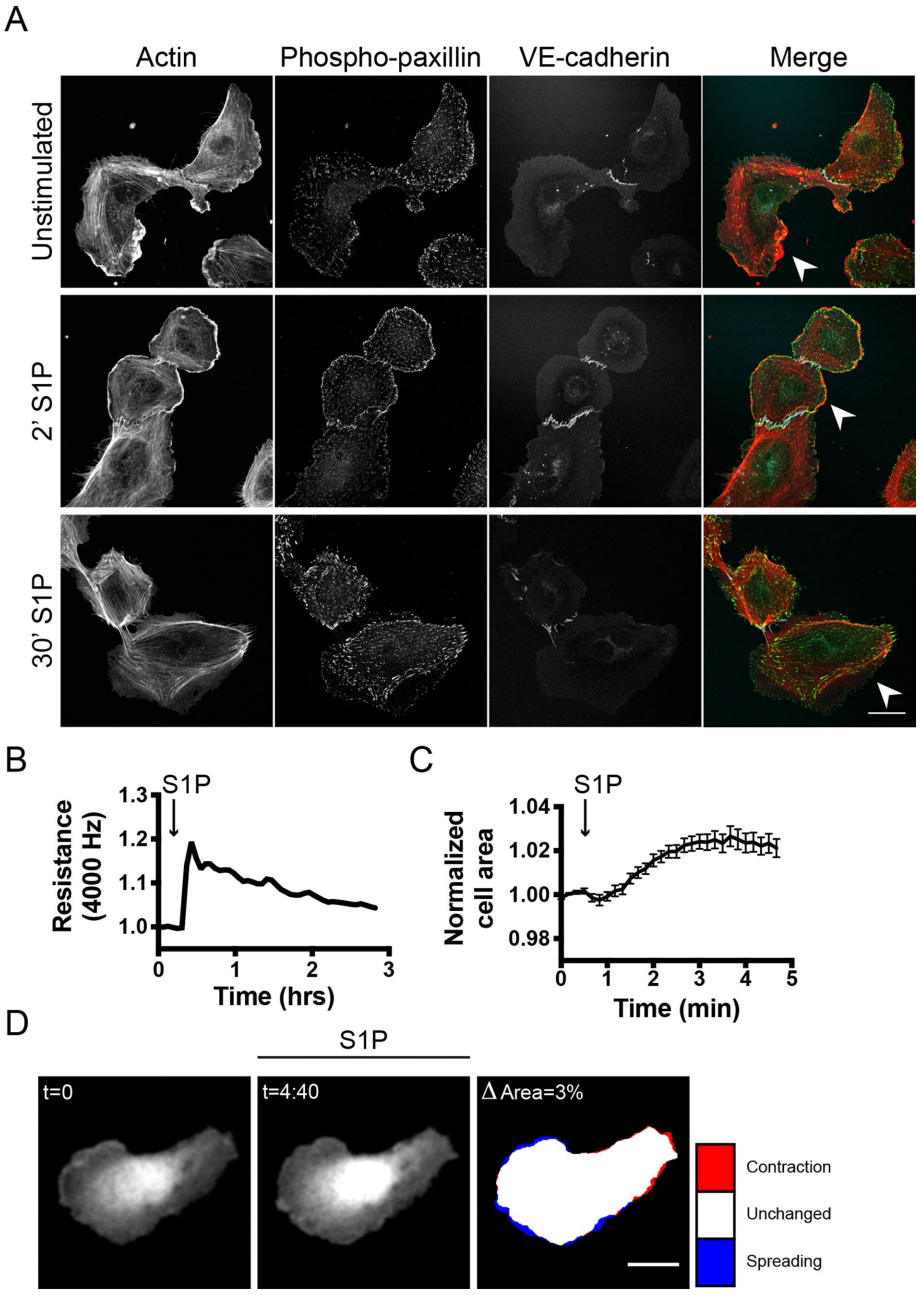

FIGURE 1: S1P promotes endothelial barrier function: analysis toward a single cell level. (A) ECs were grown to a semiconfluent monolayer, stimulated with S1P (500 nM), and stained for F-actin, phospho-paxillin, and VE-cadherin. Arrowheads highlight protruding areas. Scale bar = 25 μm. (B) ECs were grown to a monolayer on ECIS electrodes and stimulated with S1P at t = 0.3 h. Endothelial resistance (4000 Hz) was measured using the ECIS, normalized to the value at t = 0, and plotted versus time. (C) ECs, transiently transfected with mTq2, were grown to a monolayer. Local changes in the area of a single cell were measured before and after stimulation with S1P at t = 0:30 min. Graph displays a representative dataset of n = 9. (D) Corresponding image of the plot in C. Colors in the right image represent area change after S1P stimulation (look-up table panel on the right). Scale bar = 25 μm.

a monolayer demonstrated an average net 2.6% increase in cell area upon S1P addition (Figure 1C). Detailed imaging of local changes in morphology, however, showed that some parts of the cells contracted while other parts spread in response to S1P (Figure 1D and Supplemental Figure S1).

Collectively, these data show that the barrier-promoting effect of S1P on monolayers of ECs is a composite response composed of F-actin reorganization, FA redistribution, and localized spreading as well as contraction.

S1P activates different RhoGTPases that are linked to EC morphology changes

Our results demonstrated that S1P-mediated endothelial barrier promotion is not exclusively linked to cell spreading. To explore the molecular mechanisms behind this observation, we specifically focused on RhoGTPases. This group of proteins has been strongly linked to cell morphology regulation (Jaffe and Hall, 2005; Ridley, 2006) and has been previously implicated in S1P-mediated endothelial barrier regulation.

Previous studies have reported detection of S1P-induced activation of the RhoGTPases Rac1, Cdc42, and RhoA in ECs using biochemical approaches (Vouret-Craviari *et al.*, 2002; Breslin *et al.*, 2015). Here we set out to extend these observations by including the closely RhoA-related GTPases RhoB and RhoC in our analysis. Using a Cdc42/Rac interactive binding (CRIB) peptide–based pull-down assay, we found that Rac1 and Cdc42 showed immediate activation after stimulation with S1P (0.5 min; Figure 2, A and B). More persistent Rac1 activation was also observed at 2, 5, 10 and 30 min of stimulation (Figure 2A). Highest Cdc42 activation was observed at t = 2 min, with a decline at later time points (5, 10, and 30 min; Figure 2B). In addition to Rac1 and Cdc42 activation, an increase in RhoA/B/C activation was observed after 0.5 min of S1P stimulation, and for RhoA/C, but not RhoB, activation decreased again at t = 2 min (Figure 2, C–E).

Because we observed parallel activation of the three major RhoGTPases upon S1P addition, we studied the connection between the activation of these proteins and specific EC morphological changes. To this end, we used rapamycin-induced membrane recruitment (Putyrski and Schultz, 2011) of an ectopically expressed RhoGEF, which induces endogenous RhoGTPase activation upon translocation to the PM. Catalytic guanine exchange factor (GEF) domains of either p63RhoGEF (an activator of RhoA/B/C) or TIAM (an activator of Rac1) were fused to an FKBP12 domain and tagged with a fluorescent protein to examine their localization. In addition, we cotransfected Lck-FRB-ECFP, a membrane-anchored FKBP12-binding protein tagged with cyan fluorescent protein (CFP). Upon rapamycin addition, the FKBP12-GEF relocated to Lck-FRB-ECFP at the PM (Figure 2F and Supplemental Movie S1). Recruitment of TIAM predominantly induced cell expansion (ΔArea: 22%; Figure 2G and Supplemental Figure S2A), which is in line with

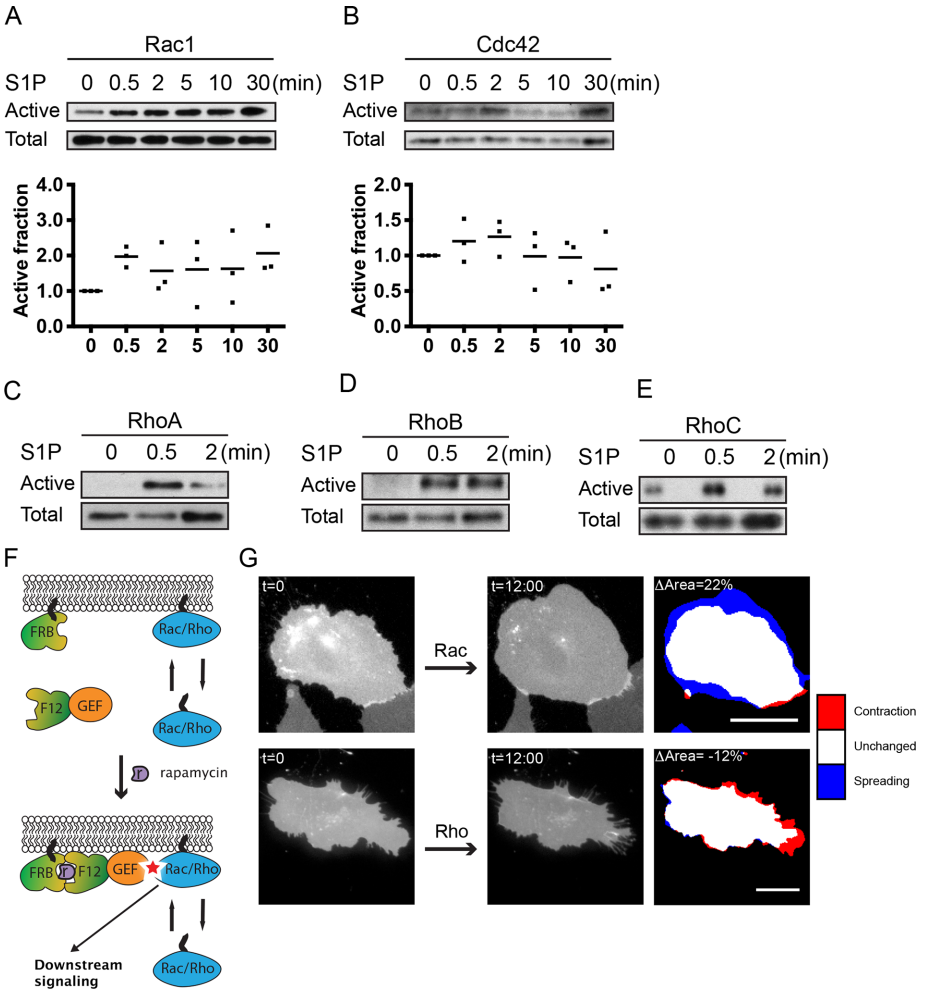

FIGURE 2: S1P activates different RhoGTPases, in line with EC morphology changes. (A, B) Rac1- and Cdc42-guanosine triphosphate (GTP) levels were increased after S1P (500 nM) stimulation, as measured by a CRIB peptide–based pull-down approach. Total protein levels of corresponding RhoGTPases were measured to control for equal loading. (C–E) RhoA-, RhoB-, and RhoC-GTP levels were increased after S1P (500 nM) stimulation, as measured by a rhotekin-RBD pull-down approach. Total protein levels of the corresponding RhoGTPases were measured to control for equal loading. (F) A rapamycin-dependent recruitment system was used to directly activate RhoGTPases. FRB, Lck-FRB-ECFP; F12, FKBP12-mCherry; GEF, either p63RhoGEF to induce RhoA activation or TIAM to induce Rac1 activation. (G) Application of the rapamycin-dependent system described in F. Rac1 activation via recruitment of TIAM induced an increase in cell area, while p63RhoGEF-mediated activation of Rho induced a decrease in cell area. Colors in the right image represent area changes (look-up table panel on the right). Scale bar = 20 μm.

the activation of Rac1. In contrast, recruitment of p63RhoGEF resulted in cell contraction (ΔArea: –12%), which is in line with the activation of RhoA/B/C GTPases (Figure 2G and Supplemental Figure S2B). These effects on EC morphology were more pronounced as compared with S1P-mediated EC morphology changes (compare Figure 1D and Figure 2G), probably because relocation of constitutive active GEF proteins provides a stronger effect on RhoGTPases than activation of endogenous GEFs by a receptor-mediated signal.

In summary, we showed prominent S1P-mediated activation of different RhoGTPases, that is, Rac1, Cdc42, and RhoA/B/C. In addition, we could directly link changes in EC morphology to RhoGTPase activation by selective GEFs, namely Rac1-mediated spreading through expression of TIAM and Rho-mediated contraction through expression of p63 RhoGEF.

S1P induces spatiotemporal control of RhoGTPase activation

Although we showed S1P-mediated activation of RhoGTPases, our biochemical approach lacks spatial information and has poor temporal resolution. In addition, quantification of these biochemical assays is challenging. To study S1P-mediated signaling with high spatiotemporal resolution, we used RhoGTPase FRET sensors. These unimolecular FRET sensors have been previously described (Lin *et al.*, 2015; Timmerman *et al.*, 2015; van Unen *et al.*, 2015; Kedziora *et al.*, 2016; Reinhard *et al.*, 2016) and can monitor fast yellow fluorescent protein (YFP)/CFP ratio differences in different cellular locations. An increase in YFP/CFP ratio corresponds to an increase in RhoGTPase activation.

Sensor-expressing primary human ECs were grown to confluency and stimulated with S1P at t = 1:50 min after the initiation of imaging. Rac1, Cdc42, and RhoA/B/C FRET sensors all showed activation in response to S1P, with the majority of the signal localized to the periphery of the cells (Figure 3A and Supplemental Figure S3). More detailed analysis of these FRET sensor experiments revealed striking temporal differences in RhoGTPase activation that could not be detected on Western blot (compare Figure 2, A–E, and Figure 3, A and B). After S1P addition, a fast decrease (reaching a minimum 1:00 min after S1P addition) in Rac1 activation was observed, followed by an increase that reached its maximum (YFP/CFP_{max}) 3:50 min after addition of S1P. Of note, measuring 32 single Rac1 sensor-expressing cells revealed two different populations of responders (Supplemental Figure S4). In addition to a population of cells (18 out of 32) with similar kinetics as the overall mean (n = 18), a second population showed a comparable initial decrease in Rac1 activation but never reached a YFP/CFP_{max} above baseline (n = 14). In contrast to Rac1, maximal FRET changes were detected at earlier time points for Cdc42 (0:40 min after addition) and RhoA (0:30 min after addition). In addition, a second Cdc42 activation peak at 3:00 min after S1P addition was detected. Zooming in on the first 7 min of the FRET sensor analyses of Figure 3B highlights the notion that the fast peak in Cdc42 and RhoA activation coincides with the initial reduction in Rac1 activation (first dashed line in Figure 3C). In addition, the second Cdc42 activation peak coincides with the delayed increase in Rac1 activation (Figure 3C, second dashed line).

Overall these data show that S1P triggers differential spatiotemporal activation of Rac1, Cdc42, and RhoA. The time course of S1P-induced (in)activation of Rac1 is a mirror image of the S1P-induced transient activation of RhoA. In contrast to Rac1, Cdc42 is activated at 0:40–3 min with similar kinetics as RhoA. However, while RhoA is inactivated after 2–5 min of stimulation, Cdc42

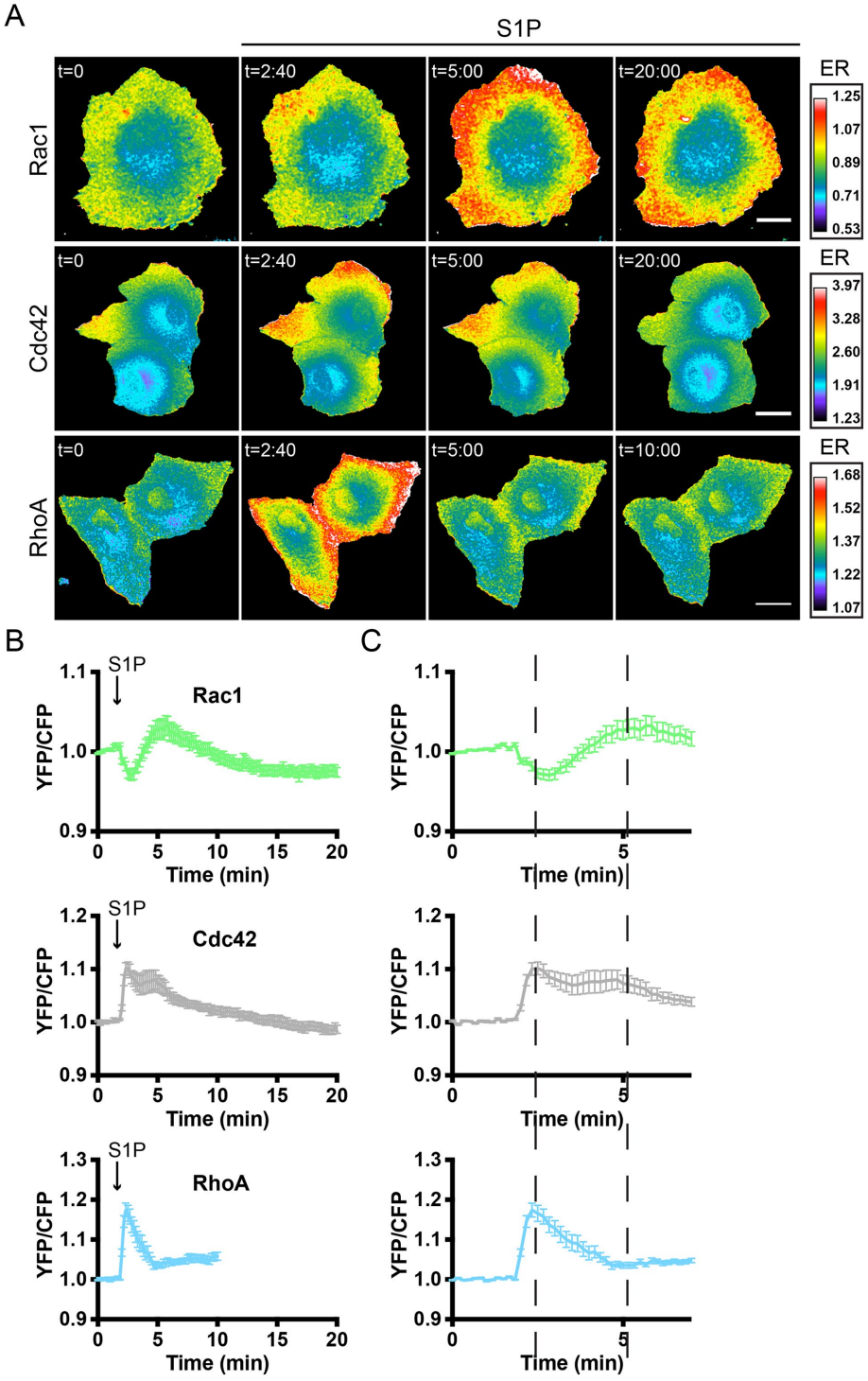

FIGURE 3: S1P induces spatiotemporal control of Rac1, Cdc42, and RhoA activation. (A) Ratiometric images of ECs that were transfected with the Rac1, Cdc42, or RhoA FRET sensor and stimulated with S1P (500 nM) at $t = 1$ min, 50 s. Warm colors represent high activation (high YFP/CFP ratios) and correspond to the emission ratios (ERs) on the right. Scale bar = 15 µm for Rac1 and 25 µm for Cdc42 and RhoA images. (B) Normalized mean YFP/CFP ratio traces (±SEM) for Rac1 ($n = 32$), Cdc42 ($n = 19$), and RhoA ($n = 12$) FRET sensor-expressing ECs before and after stimulation with S1P. (C) Zoom of normalized mean YFP/CFP ratio traces (±SEM) corresponding to the first 7 min of the traces in B. Dashed lines highlight maximal and minimal changes in YFP/CFP ratios for the different GTPases (see section *S1P induces spatiotemporal control of RhoGTPase activation*).

shows more persistent activation. Thus, all three GTPases show distinct (in)activation profiles in response to S1P.

S1P activates $G\alpha_i$ and $G\alpha_{13}$ but not $G\alpha_q$

The FRET sensor data revealed a rapid (in) activation of the three major RhoGTPases. To understand how the regulation of RhoGTPase activity is orchestrated, we examined receptor-proximal events. S1P binds various GPCRs, initiating intracellular signaling events via activation of different heterotrimeric G-proteins. To examine which of these G-proteins are activated by S1P, we used dedicated FRET-based biosensors that have recently been developed in our lab (Goedhart *et al.*, 2011; van Unen *et al.*, 2016).

The heterotrimeric G-protein sensors use a Gα subunit tagged with a donor and a Gγ2 subunit tagged with an acceptor. The intact complex in resting cells shows FRET, which is lost upon activation. This means that a decrease in YFP/CFP ratio corresponds to an increase in G-protein activation (Figure 4A, representing a schematic on the working mechanism of these sensors). We recently showed that S1P strongly activates the $G\alpha_i$ protein in ECs (van Unen *et al.*, 2016). However, according to published literature, both $G\alpha_{13}$ and $G\alpha_q$ also play a role in S1P-mediated signaling in ECs (Poti *et al.*, 2014). To measure activation of $G\alpha_{13}$, we made use of a new sensor (M.M. and J.G., unpublished data) that comprised a $G\alpha_{13}$ subunit tagged with mTq2 as the donor and a YFP-tagged Gγ2 subunit as the acceptor. First, we characterized the $G\alpha_{13}$ sensor by stimulating ECs with thrombin, a well-known $G\alpha_{13}$ activator (Offermanns *et al.*, 1994; Barr *et al.*, 1997; Marinissen *et al.*, 2003). Stimulation of $G\alpha_{13}$ FRET sensor-expressing ECs induced a FRET ratio change distributed throughout the entire cell, reaching a YFP/CFP_{max} (–17%) 25 s after thrombin stimulation (Figure 4B). The observation that the new sensor responds to stimulation of an endogenous GPCR suggests that the $G\alpha_{13}$ FRET sensor can be used as a robust and sensitive read-out of $G\alpha_{13}$ activation.

Compared with thrombin activation, similar $G\alpha_{13}$ spatiotemporal activation kinetics were detected after stimulation with S1P, reaching YFP/CFP_{max} (–11%) 20 s after stimulation (Figure 4C). Surprisingly, S1P stimulation did not induce $G\alpha_q$ activation in $G\alpha_q$ sensor-expressing cells (Figure 4D). In contrast, the well-known $G\alpha_q$ activator

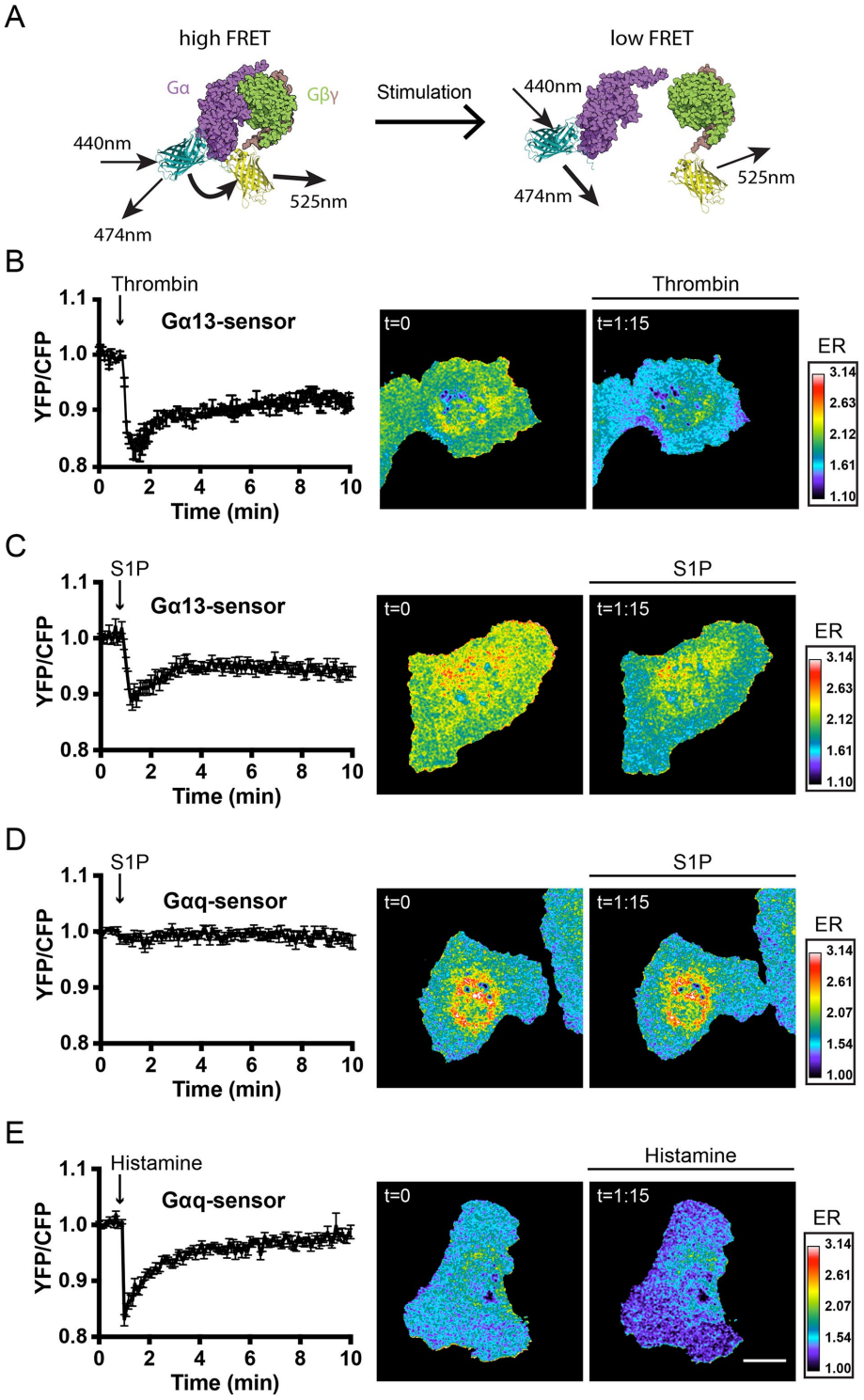

FIGURE 4: S1P induces $G\alpha_{13}$ but not $G\alpha_q$ activation. (A) G-protein FRET sensor design, consisting of (from N- to C-terminus) Gβ-2A-YFP-$G\gamma_2$-IRES-Gα-mTq2 (Goedhart *et al.*, 2011; van Unen *et al.*, 2016). (B) Normalized mean YFP/CFP ratio traces (±SEM) of $G\alpha_{13}$ FRET sensor-expressing ECs ($n = 6$) stimulated with thrombin (1 U/ml) at $t = 55$ s, including ratiometric images of the indicated time points (similar in C–E). (C) Normalized mean YFP/CFP ratio traces (±SEM) of $G\alpha_{13}$ FRET sensor-expressing ECs ($n = 14$) stimulated with S1P (500 nM) at $t = 55$ s. (D) Normalized mean YFP/CFP ratio traces (±SEM) of $G\alpha_q$ FRET sensor-expressing ECs ($n = 12$) stimulated with S1P (500 nM) at $t = 55$ s. (E) Normalized mean YFP/CFP ratio traces (±SEM) of $G\alpha_q$ FRET sensor-expressing ECs ($n = 10$) stimulated with histamine (100 μM) at $t = 55$ s. Blue colors represent high activation (low YFP/CFP ratios) and correspond to the emission ratios (ERs) on the right. Scale bar = 20 μm.

histamine showed fast and robust $G\alpha_q$ activation (–17% YFP/CFP_{max} 5 s after histamine stimulation; Figure 4E). Taken together, these G-protein FRET sensor experiments reveal that, in addition to $G\alpha_i$, the G-protein $G\alpha_{13}$ but not $G\alpha_q$ is activated by S1P in ECs.

The $S1P_1$ receptor exclusively signals toward $G\alpha_i$, Rac1, and Cdc42

To study the link between heterotrimeric G-protein and RhoGTPase signaling, we wanted to use a method to activate only $G\alpha_i$-mediated signaling. The compound SEW2871 is reported as a specific agonist for the $S1P_1$ receptor and activator of $G\alpha_i$. Like S1P, SEW2871 stimulation resulted in an increase in transendothelial electrical resistance as measured by ECIS (Figure 5A). In addition, SEW2871 showed robust $G\alpha_i$ activation within 1 min of stimulation (Figure 5B). No SEW2871-induced changes in $G\alpha_{13}$ activation could be detected (Figure 5C).

Because SEW2871 appeared to exclusively signal toward $G\alpha_i$, we next explored its signaling toward the GTPases Rac1, Cdc42, and RhoA. After addition of SEW2871, increases in Rac1 and Cdc42 activation were observed, while RhoA sensor-expressing ECs did not show a change in FRET (Figure 5D). In contrast to S1P-induced Rac1 activation, activation of Rac1 by SEW2871 was not preceded by Rac1 inactivation, indicating that the rapid inactivation of Rac1 by S1P is mediated by RhoA. In addition, comparing the activation of Rac1 and Cdc42 showed Cdc42 activation at 1–3 min after stimulation, whereas Rac1 activation is maximal at 4–5 min after stimulation, showing similar dynamics as the S1P-mediated activation (compare Figure 5, D and E, with Figure 3, B and C). In summary, the endothelial barrier-promoting compound SEW2871 acts through $G\alpha_i$, Rac1, and Cdc42 but does not activate RhoA.

$G\alpha_i$ signaling pathways are required for S1P-mediated endothelial barrier stimulation

The responses of ECs to SEW2871 suggest that $G\alpha_i$ determines S1P signaling toward Rac1 and Cdc42. We therefore explored whether Rac1 and/or Cdc42 activation exclusively depends on $G\alpha_i$ and to what extent this regulates S1P-mediated barrier regulation in ECs. To block signaling through $G\alpha_i$, we used pertussis toxin (PTX). This toxin selectively ADP-ribosylates $G\alpha_i$, abolishing its activation. ECs, transiently expressing the Rac1, Cdc42, or RhoA sensor, were treated

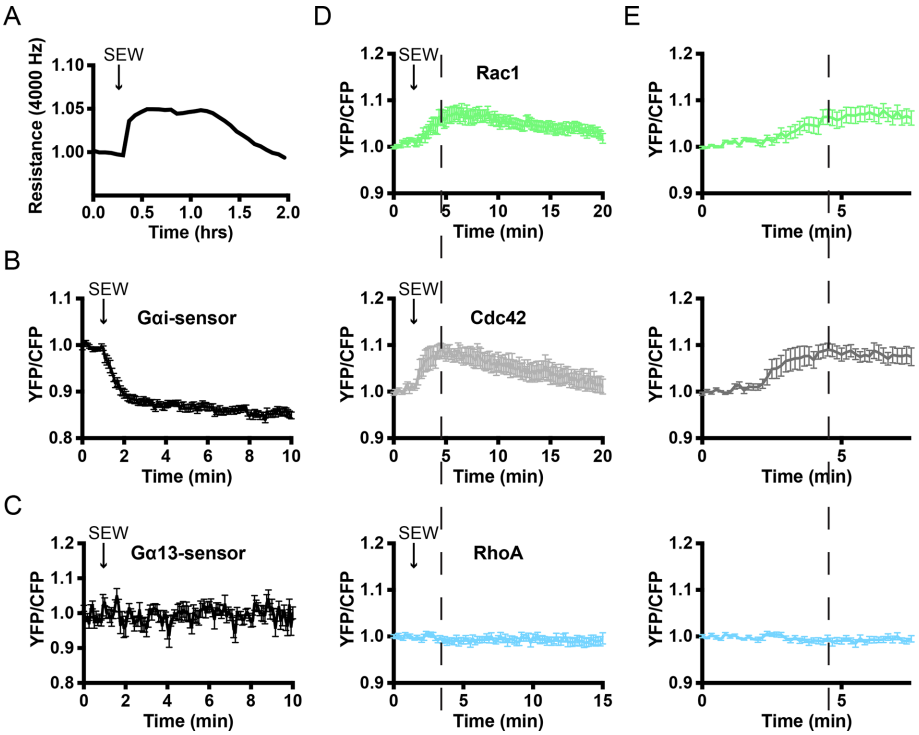

FIGURE 5: SEW2871 promotes endothelial barrier function and activates $G\alpha_i$, Rac1, and Cdc42. (A) ECs were grown to a monolayer on ECIS electrodes and stimulated with SEW2871 (5 μM) at $t = 0.3$ h after start of the analysis. Endothelial resistance (4000 Hz) was measured using the ECIS. (B) Normalized mean YFP/CFP ratio traces (±SEM) of $G\alpha_i$ FRET sensor-expressing ECs ($n = 14$) stimulated with SEW2871 (5 μM) at $t = 55$ s. (C) Normalized mean YFP/CFP ratio traces (±SEM) of $G\alpha_{13}$ FRET sensor-expressing ECs ($n = 16$) stimulated with SEW2871 (5 μM) at $t = 55$ s. (D) Normalized mean YFP/CFP ratio traces (±SEM) for Rac1 ($n = 16$), Cdc42 ($n = 8$), and RhoA ($n = 6$) FRET sensor-expressing ECs before and after stimulation with SEW2871 (5 μM) at $t = 1$ min, 50 s. (E) Zoom of normalized mean YFP/CFP ratio traces (±SEM) corresponding to the first 7 min of D. Dashed lines highlight maximal YFP/CFP ratio changes of Rac1 and Cdc42.

with PTX for at least 18 h before stimulation with S1P. PTX-treated ECs lacked both Rac1 and Cdc42 activation after stimulation with S1P, while the fast Rac1 inactivation remained detectable (Figure 6, A and B). RhoA sensor-expressing and PTX-pretreated ECs still showed prominent S1P-induced activation after pretreatment with PTX (Figure 6C), and a prolonged response was observed compared with untreated ECs (compare B and C in Figure 3). This suggests that the RhoA inactivation, observed in untreated cells 1–4 min after S1P, is mediated by a Rac1/Cdc42-dependent signaling pathway.

As for the endothelial barrier function, the effect of $G\alpha_i$ inhibition was studied by using the ECIS. Control and PTX-treated endothelial monolayers were stimulated with S1P, where PTX-treated cells started at a slightly lower baseline level (Supplemental Figure S5). Control cells showed a barrier-promoting response similar to that described above (Figure 1B). Strikingly, a substantial loss of endothelial barrier integrity was observed upon S1P stimulation of PTX-treated cells (Figure 6D). The observed decrease in barrier function returned to baseline with the same kinetics as the control (Figure 6D). This reversed effect on the endothelial barrier was also observed in PTX-treated ECs analyzed by immunostaining. Unstimulated ECs in a semiconfluent cell layer, and treated with PTX, predominantly showed a contractile phenotype with disruption of the junctional VE-cadherin complex (Figure 6E). In contrast to what we have seen in Figure 1A, S1P stimulation did not result in increased cell protrusion (compare Figure 1A and Figure 6E). Moreover, increased levels of stress fibers and enlarged phospho-paxillin–positive FAs were observed after stimulation with S1P, indicating that a contractility-regulating (i.e., RhoA-driven) pathway becomes dominant over a cell-spreading (i.e., Cdc42/Rac1-driven) pathway in PTX-treated ECs.

Collectively, these data suggest that $G\alpha_i$ is specifically linked to Rac1 and Cdc42 activation and that this pathway is dominant in S1P-stimulated ECs, promoting endothelial barrier function.

Specific $G\alpha_{13}$ inhibition affects Rac1 and RhoA but not Cdc42 signaling

Although $G\alpha_i$ is required for Rac1/Cdc42 activation and for the S1P-induced increase in endothelial barrier function, the role of $G\alpha_{13}$ signaling in S1P signaling is unexplored. Because no pharmacological inhibitors have been reported for $G\alpha_{13}$, a different strategy was required to specifically inhibit this type of G-protein. Therefore, we used p115RhoGEF, a specific RhoGEF that becomes activated in $G\alpha_{13}$-mediated signaling pathways (Hart *et al.*, 1998). In addition to its GEF activity toward RhoGTPases, p115RhoGEF acts as a GTPase activating protein (GAP) for $G\alpha_{13}$ proteins via its so-called regulator of G-protein signaling (RGS) domain (Sternweis *et al.*, 2007). p115-RGS accelerates intrinsic $G\alpha_{13}$ GTPase activity, thereby selectively blocking the activation of $G\alpha_{13}$-coupled GPCRs.

To use the p115-RGS domain to inhibit $G\alpha_{13}$-mediated signaling, p115-RGS was cloned from full-length p115RhoGEF and tagged with the mCherry-fluorescent protein. We created three different versions of tagged p115-RGS: C-terminal tagged (p115-RGS-mCherry), N-terminal tagged (mCherry-p115-RGS), and membrane-linked, N-terminal tagged (Lck-mCherry-p115-RGS). To test the efficiency of $G\alpha_{13}$ inactivation of these constructs, RhoA sensor-expressing HeLa cells were cotransfected with $G\alpha_{13}$-QL (a constitutively active $G\alpha_{13}$ mutant) and/or the different p115-RGS constructs. Compared with control cells, overexpression of $G\alpha_{13}$-QL induced an increase in RhoA activation (Supplemental Figure S6). Although all three p115-RGS constructs diminished this $G\alpha_{13}$-QL–mediated increase in RhoA activation, Lck-mCherry-p115-RGS was the most efficient (Supplemental Figure S6).

Next, the effect of $G\alpha_{13}$ inhibition was studied on S1P-mediated RhoGTPase activation. In Rac1 sensor-expressing ECs, cotransfection with either Lck-mCherry or Lck-mCherry-p115-RGS showed a similar increase in S1P-induced Rac1 activation. Intriguingly, Lck-mCherry-p115-RGS cotransfected cells showed a less-pronounced Rac1 inactivation drop at 3–5 min as well as a higher maximal FRET ratio. In contrast, Lck-mCherry-p115-RGS almost completely inhibited S1P-induced RhoA activation, whereas no effect on Cdc42 activation was observed (Figure 7, A and B)

Taken together, these experiments demonstrated that membrane-linked p115-RGS efficiently inhibits $G\alpha_{13}$-mediated signaling and S1P-induced activation of RhoA. This inhibition of RhoA activation was also reflected in increased and more sustained Rac1 activation, while Cdc42 remained unaffected. These data, in combination with

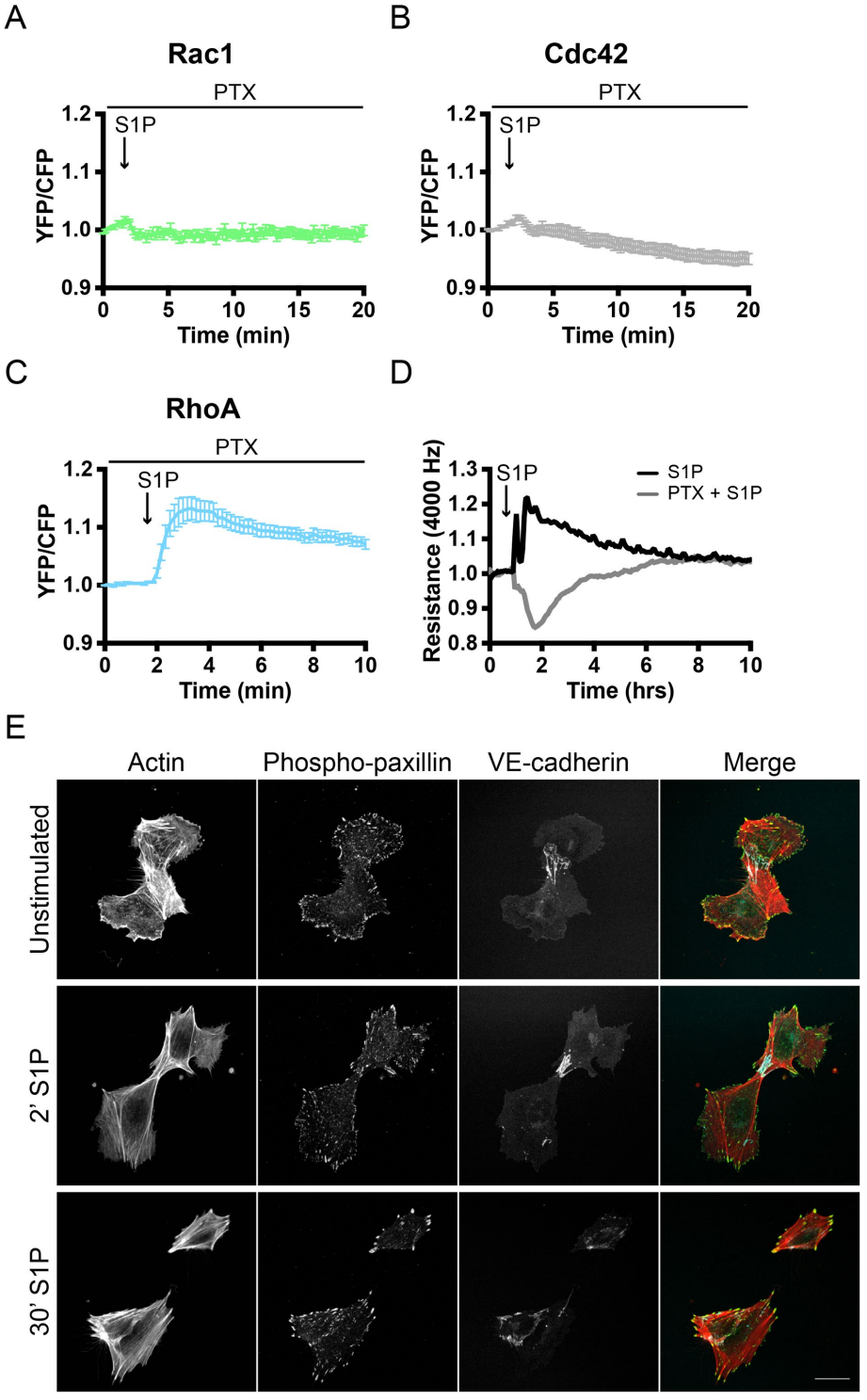

FIGURE 6: $G\alpha_i$ signaling is required for S1P-mediated Rac1/Cdc42 activation and endothelial barrier promotion. (A–C) Normalized mean YFP/CFP ratio traces (±SEM) for Rac1 ($n = 12$), Cdc42 ($n = 9$), and RhoA ($n = 13$) FRET sensor-expressing ECs (pretreated with 100 ng/ml PTX) before and after stimulation with S1P (500 nM) at $t = 1{:}50$. (D) ECs were grown to a monolayer on ECIS electrodes, pretreated with water or PTX dissolved in water (100 ng/ml), and stimulated with S1P (500 nM) at $t = 50$ min. Endothelial resistance (4000 Hz) was measured using the ECIS. (E) EC were grown to a semiconfluent monolayer, pretreated with PTX as above, stimulated with S1P (500 nM), and stained for F-actin, phospho-paxillin, and VE-cadherin. Scale bar = 25 μm.

the findings presented in Figures 3–6, further support the notion that in ECs, Rac1 and RhoA mutually inhibit each other, whereas Cdc42 is activated by a Cdc42-selective GEF and is insensitive to RhoA-mediated inhibitory cross-talk (Figure 7C).

DISCUSSION

This study reveals that the integrated activity of RhoA, Rac, and Cdc42 determines the effect of S1P on EC morphology and endothelial barrier function. We have uncovered a link between the activity of specific heterotrimeric G-proteins and RhoGTPases in ECs. Furthermore, we link the activity of individual RhoGTPases to EC morphology. Our results provide evidence for a model (Figure 7C) in which S1P activates two pathways in ECs that have opposing effects on cell morphology. On the one hand, the $S1P_1$ receptor couples to $G\alpha_i$ and consequently activates both Rac1 and Cdc42, albeit with different kinetics and most likely through different GEFs. On the other hand, RhoA is activated, most likely via the $S1P_2$ receptors that signal toward $G\alpha_{13}$. The balance between these pathways is determined at the level of the receptors or the heterotrimeric G-proteins and determines the effect of S1P on cell shape and ultimately barrier function. Our study implies that the relative expression of S1P receptor isoforms and heterotrimeric G-proteins determines the signaling outcome. Under native conditions, the Rac1/Cdc42-based signaling dominates, leading to a net increase in cell spreading and increased barrier function in endothelial monolayers. However, under specific (patho) physiological conditions, altered receptor levels may change the signaling outcome.

Previous studies on S1P signaling in ECs, mainly focused on barrier regulation of endothelial monolayers, showed that S1P stimulation promotes vascular stability. Intriguingly, several biochemical experiments have revealed S1P-mediated activation of the most well-studied GTPases Rac1, Cdc42, and RhoA in ECs (Vouret-Craviari *et al.*, 2002; Breslin *et al.*, 2015). Both the barrier-promoting effect of S1P and the activation of the three types of Rho GTPases by pull-down assay on cell extracts were corroborated in this study.

The barrier-promoting effect was measured using ECIS. However, ECIS lacks spatial information and details on the molecular mechanisms underlying morphological changes. Our biochemical approach that measures active Rho GTPases, showing S1P-dependent activation of different

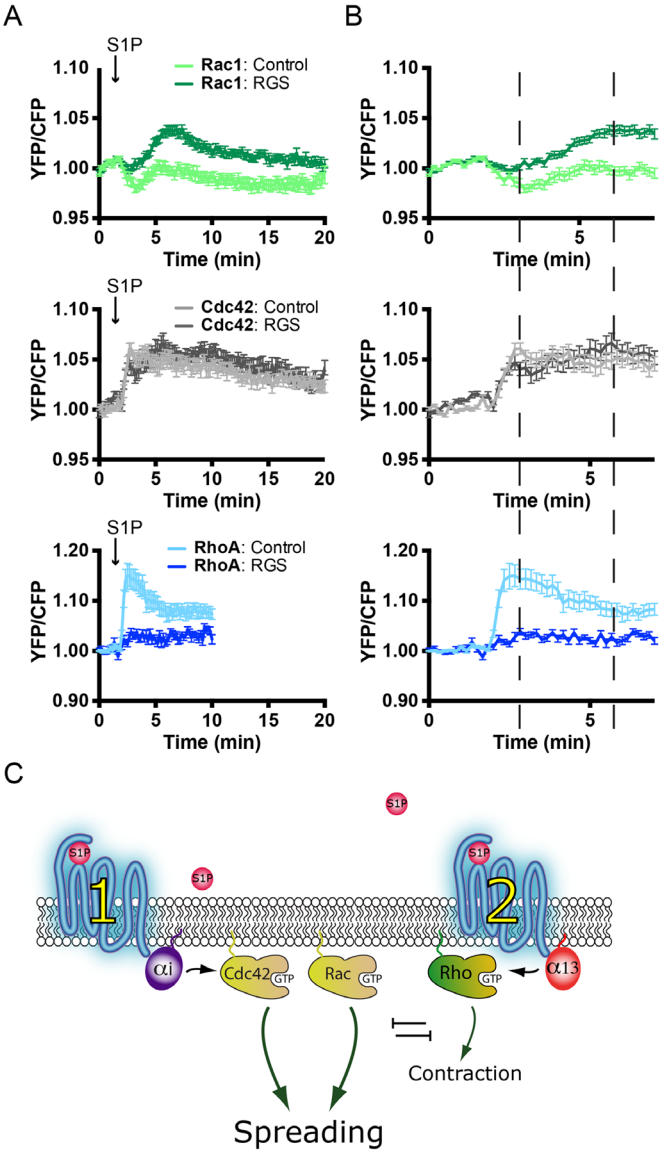

FIGURE 7: $G\alpha_{13}$ inhibition enhances S1P-induced Rac1 activation and blocks RhoA activation. (A) Normalized mean YFP/CFP ratio traces (±SEM) for Rac1, Cdc42, and RhoA FRET sensor-expressing ECs before and after stimulation with S1P at $t = 1$ min, 50 s. FRET sensor–positive ECs coexpress either Lck-mCherry (control) (Rac1, $n = 20$; Cdc42, $n = 21$; RhoA, $n = 14$) or Lck-RGS-mCherry (RGS) (Rac1, $n = 27$; Cdc42, $n = 22$; RhoA, $n = 14$). (B) Enlargement of normalized mean YFP/CFP ratio traces (±SEM) corresponding to the first 7 min of A. Dashed lines highlight maximal and minimal YFP/CFP ratio changes. Note the increased Rac1 activation at ~7 min and the inhibition of RhoA activation upon coexpression of the RGS domain. (C) Model describing S1P-mediated signaling pathways in ECs. Balancing G-protein and RhoGTPase signaling results in S1P-induced cell spreading, which dominates over the limited RhoA activation and consequent contraction.

RhoGTPases, lacks spatial information, has low temporal resolution, and is difficult to quantify with some precision. Furthermore, both assays require large cell numbers, thereby completely lacking detection of cell-to-cell variation.

To circumvent the limitations of the aforementioned approaches, we undertook detailed analysis of RhoGTPase activation in space and time by performing single-cell FRET measurements. By using recently developed and validated single-chain RhoGTPase FRET sensors (Lin *et al.*, 2015; Timmerman *et al.*, 2015; van Unen *et al.*, 2015; Kedziora *et al.*, 2016; Reinhard *et al.*, 2016), we visualized robust activation and differences in activation profiles between Rac1, Cdc42, and RhoA/B/C. Here, we show that upon S1P stimulation, Rac1 is initially inactivated and that this inactivation is paralleled by increase in RhoA activation, suggesting that RhoA suppresses Rac1 activity (in line with previous studies in a different context, which are reviewed in Burridge and Doughman [2006]). The observed RhoA activation can explain the observed local contraction (Figure 1D). In contrast to Rac1 and parallel to RhoA, Ccd42 shows a rapid activation, which also correlated well with the fast barrier-protective effect of S1P, which was detected using ECIS. The observation that the earliest response to S1P, that is, a rapid increase in barrier function, is paralleled by activation of Cdc42 and RhoA and inhibition of Rac1 suggests that Cdc42 is the most relevant GTPase mediating this initial stabilizing effect on cell–cell junctions, overruling RhoA-mediated contractility. Based on the distinct Rac1 and Cdc42 activation profiles and our findings using the $S1PR_1$ agonist SEW2871, we hypothesize that different GEFs and GAPs are involved in these responses: a Cdc42-specific GEF and RhoA-dependent, Rac1-specific GAP during the initial activation at 1–3 min and one or more Cdc42/Rac1 GEF(s), which ensure activation of both GTPases at ~4–7 min, in conjunction with a RhoAGAP, which downregulates RhoA activation. Future research is warranted to define how a single S1P receptor can activate different GEFs sequentially, an effect possibly related to receptor dimerization, feedback loops, or internalization, inducing a time delay in downstream signaling.

The activities of Rac1, Cdc42, and Rho GTPases in S1P signaling are orchestrated by upstream events. Three different GPCRs ($S1PR_1$, $S1PR_2$, and $S1PR_3$) initiate S1P signaling in ECs and have been hypothesized to couple to different heterotrimeric G-proteins, $G\alpha_i$, $G\alpha_{13}$, and $G\alpha_q$. For the first time, to our knowledge, we have been able to directly measure, using a newly developed $G\alpha_i$ FRET sensor (van Unen *et al.*, 2016), S1P-induced $G\alpha_i$ activation in single human ECs. A novel FRET-based sensor based on the same design (M.M. and J.G., unpublished data) was sensitive enough to detect thrombin-mediated activation of $G\alpha_{13}$ in ECs. By using FRET sensors for $G\alpha_{13}$ or $G\alpha_q$, we observed that $G\alpha_{13}$ but not $G\alpha_q$ is activated by S1P. Together, our data show that S1P-mediated barrier regulation in human endothelium is predominantly controlled by $G\alpha_i$ and $G\alpha_{13}$. The specific $S1PR_1$ agonist SEW2871 furthermore shows exclusive coupling to $G\alpha_i$, resulting in activation of Rac1 and Cdc42 but not RhoA. We observed neither initial Rac1 inactivation nor RhoA activation in response to this $S1PR_1$-$G\alpha_i$ activation, underlining the antagonistic properties of RhoA toward Rac1 in the early phase after S1P activation.

Inhibition of $G\alpha_i$ by PTX abolished S1P-induced Rac1/Cdc42 activation. This indicates that Rac1/Cdc42 activation is not only mediated but also restricted to $G\alpha_i$ signaling. The lack of $G\alpha_i$-Rac1/Cdc42 signaling furthermore results in dominant RhoA signaling, as shown by prolonged RhoA FRET signals showing a lack of RhoA inactivation. $G\alpha_i$ inhibition has a striking effect on signaling outcome, completely reversing the S1P responses in the ECIS (i.e., loss rather than gain of barrier function). At a cellular level, the inhibition of $G\alpha_i$ results in S1P-induced cell contraction, explaining the loss of barrier function observed in ECIS. Inhibition of $G\alpha_i$ thus shifts S1P signaling toward an output dominated by RhoA, suggesting that S1P-mediated barrier regulation is determined at the level of the heterotrimeric G-proteins and their activating receptors. Whereas $G\alpha_i$ regulates sequential activation of Cdc42 and Rac1, $G\alpha_{13}$ exclusively and rapidly activates Rho signaling and consequent cell contraction.

GPCRs may activate multiple different heterotrimeric G-proteins (Wettschureck and Offermanns, 2005), either via a single GPCR or via multiple GPCRs that activate different heterotrimeric G-proteins but react to the same ligand, as is the case for S1P receptors. Because we demonstrate that the output of such networks can be explained only by observing multiple parameters, our results have important implications for understanding signaling networks activated by GPCRs. Ideally, multiple events are measured at the same time by multiparameter imaging (Welch *et al.*, 2011), and this remains a challenge for the future. The FRET-based sensors used in this study for heterotrimeric G-proteins and RhoGTPases have proven to be valuable tools for dissecting the complexity of signaling networks in primary cells.

The effects of S1P are generally assumed to promote endothelial integrity and vascular stability. However, it is important to note that the outcome of S1P-induced signaling may divert from this generic response: vascular beds may affect the outcome of this signaling, and signaling outcomes may even differ among different sections of the same blood vessel (Guan *et al.*, 2014; Galvani *et al.*, 2015). Moreover, S1P in plasma is bound to carrier proteins, and differential effects of high-density lipoprotein–bound S1P versus albumin-bound S1P have been reported (Wilkerson *et al.*, 2012; Galvani *et al.*, 2015). Also, variations in S1P receptor coding sequences (Obinata *et al.*, 2014) or receptor expression levels in health and disease (Mahajan-Thakur *et al.*, 2015) may account for different outcomes of S1P-induced signaling. On top of the aforementioned layers of regulation, our results imply that the precise balance of components immediately downstream of the S1P receptor, that is, heterotrimeric G-proteins, Rho GEFs, and GAPs, provide a fine-tuning mechanism for the spatiotemporal activation patterns of the Rho GTPases and ultimately determine effects on vascular stability.

In summary, our study unravels detailed molecular characteristics of S1P-mediated signaling pathways that regulate endothelial barrier function. Using FRET-based biosensors, we performed high-resolution spatiotemporal single-cell analysis of G-protein and RhoGTPase signaling in primary human endothelium and uncovered sequential RhoGTPase activation and partial cross-talk between RhoA and Rac1 but not Cdc42. Finally, this work emphasizes the need to study S1P-based signaling pathways that regulate vascular integrity in different tissues and vascular beds.

MATERIAL AND METHODS

Plasmids

Full-length p115RhoGEF (a kind gift of P. Sternweis) was used to amplify the p115RhoGEF-RGS domain (amino acids 1–252) by PCR amplification, using forward primer 5′-GAGATCAGATCTATGGAAGACTTCGCCCGAG-3′ and either reverse primer #1 GAGATCGAATTCTTAGTTCCCCATCACCTTTTTC-3′ or reverse primer #2 GAGATCGAATTCTGTTCCCCATCACCTTTTTCCG-3′. After amplification, the PCR fragments and vectors were cut with *Bgl*II and *Eco*RI (restriction sites are underlined in the primer sequence). Next, PCR fragments were ligated into C1-mCherry, N1-mCherry, or C1-Lck-mCherry to generate C1-mCherry-RGS, N1-RGS-mCherry, and C1-Lck-mCherry-RGS. The translocatable, catalytic domain of TIAM was obtained from Addgene (plasmid #20154) and described by Inoue *et al.* (2005), and translocatable catalytic p63RhoGEF was described by van Unen *et al.* (2015). The FRET biosensors for $G\alpha_i$ (van Unen *et al.*, 2016), $G\alpha_q$ (Goedhart *et al.*, 2011), RhoA (Lin *et al.*, 2015; van Unen *et al.*, 2015), RhoB/RhoC (Reinhard *et al.*, 2016), Rac1 (Timmerman *et al.*, 2015), and Cdc42 (Kedziora *et al.*, 2016) were as described in the cited references. A sensor for $G\alpha_{13}$ was constructed by inserting mTq2 into the αB αB1 loop between the αB and αB1 helices. The tagged $G\alpha_{13}$ subunit was coexpressed with a YFP-tagged Gγ2 subunit (Goedhart *et al.*, 2011). To ascertain robust coexpression, the tagged subunits were expressed from a single plasmid as recently reported for the $G\alpha_i$ sensor (van Unen *et al.*, 2016). The engineering and full characterization will be described elsewhere (M.M. and J.G., unpublished data).

HUVEC cell culture and transfection

Primary HUVECs were acquired from Lonza (Verviers, Belgium) and seeded on culture flasks coated with fibronectin (FN). HUVECs were grown in EGM-2 medium, supplemented with SingleQuots (Lonza), and transfected at passage #4 or #5 with a Neon transfection system (MPK5000, Invitrogen) and Neon transfection kit (Invitrogen). Per transfection, 2 µg plasmid DNA was used, and a single pulse was generated at 1300 V for 30 ms. After microporation, HUVECs were grown to a monolayer on FN-coated glass coverslips.

HeLa cell culture and transfection

HeLa cells were acquired from American Type Culture Collection (Manassas, VA). Cells were cultured in DMEM (Invitrogen, Bleiswijk, Netherlands), supplemented with GlutaMAX, 10% FBS, penicillin (100 U/ml), and streptomycin (100 µg/ml). HeLa cells were seeded on 24-mm glass coverslips (Menzel-Gläser, Braunschweig, Germany) and transfected with 1 µg plasmid DNA, 4 µg polyethylamine (PEI 25,000) in water (Polysciences), and 100 µl OptiMeM (Life Technologies, Bleiswijk, Netherlands).

Reagents

S1P was from Avanti Polar Lipids, rapamycin was from LC Laboratories (Woburn, MA), thrombin (HCT-0020) was from Haematologin Technologies, histamine (H7125) was from Sigma-Aldrich, SEW2871 (10006440) was from Cayman Chemical, and PTX (PHZ1174) was from Thermo Fisher. All compounds were prepared per the manufacturers' instructions.

Antibodies

Actin-stain 555 Phalloidin (Cytoskeleton), monoclonal antibody (mAb) mouse anti–VE-cadherin/CD144 AF647 (BD PharMingen), polyclonal antibody (pAb) rabbit anti–phospho-paxillin (PY118), and secondary antibody anti-rabbit AF488 were used for immunofluorescence.

For immunoblotting, mAb mouse anti-Rac1 and –anti-Cdc42 were purchased from BD Transduction Laboratories. mAb rabbit anti-RhoA and –anti-RhoC were from Cell Signaling. pAb rabbit anti-RhoB was from Santa-Cruz Biotechnology, and mAb mouse anti-actin was purchased from Sigma. Secondary antibody, HRP-labeled goat anti-mouse, and swine anti-rabbit were obtained from Dako.

ECIS

ECIS (Applied Biophysics, New York) electrode arrays (8W10E) were preincubated with 10 mM L-cysteine (Sigma) for 5 min at 37°C and coated with FN (10 µg/ml, 0.9% NaCl [Sigma]) for ≥1 h at 37°C. After coating, HUVECs were seeded (150,000 cells per well) and grown to confluence. The electrical resistance, as a measure of endothelial barrier function, was recorded at a frequency of 4000 Hz at 37°C and 5% CO_2.

CRIB-based Rac1/Cdc42 pull-down assays

HUVECs were grown to a monolayer, stimulated as described, and washed with ice-cold phosphate-buffered saline (PBS; 1 mM $CaCl_2$, 0.5 mM $MgCl_2$). Next, cells were lysed for 5 min on ice in lysis buffer containing 50 mM Tris (pH 7.4), 0.5 mM $MgCl_2$, 500 mM NaCl, 1% (vol/vol) Triton X-100, 0.5% (wt/vol) deoxycholic acid, and 0.1% (wt/vol) SDS supplemented with protease inhibitors (Roche). Lysed cells

were cleared by centrifuging for 5 min at 14000 × *g* and incubated with biotinylated Pak1-CRIB peptide coupled to streptavidin beads (Sander *et al*., 1999). After ≥30 min of incubation at 4°C, beads were washed five times in 50 mM Tris (pH 7.4), 0.5 mM $MgCl_2$, 150 mM NaCl, and 1% (vol/vol) Triton X-100 and eluted in SDS-sample buffer containing 4% β-mercaptoethanol. Samples were analyzed by Western blot using either anti-Rac or anti-Cdc42 antibodies.

Rhotekin-Rho binding domain (RBD) pull-down assay

HUVECs were grown to a monolayer, stimulated as described, and washed with ice-cold PBS (1 mM $CaCl_2$, 0.5 mM $MgCl_2$). Next, cells were lysed for 5 min on ice in 25 mM Tris-HCl (pH 7.2), 150 mM NaCl, 10 mM $MgCl_2$, 1% NP-40, and 5% glycerol supplemented with protease inhibitors (Roche). Lysed cells were cleared by centrifuging for 5 min at 14,000 × *g* and incubated with bacterially produced glutathione *S*-transferase rhotekin-RBD beads (Sander *et al*., 1999). After ≥30 min of incubation at 4°C, beads were washed five times in the abovementioned lysis buffer and boiled in SDS-sample buffer containing 4% β-mercaptoethanol. Samples were analyzed on Western blot by using anti-RhoA, anti-RhoB, or anti-RhoC antibodies.

Confocal imaging

HUVECs were seeded on FN-coated 14-mm glass coverslips and grown to a semiconfluent monolayer. After stimulation, cells were washed with PBS (1 mM $CaCl_2$ and 0.5 mM $MgCl_2$) and fixed for 5 min in PBS (1 mM $CaCl_2$, 0.5 mM $MgCl_2$) containing 4% formaldehyde. Next, cells were permeabilized for 5 min in PBS containing 0.5% Triton X-100, followed by 20-min incubation in 0.5% PBS-bovine serum albumin (BSA) blocking buffer. Subsequently, cells were incubated for 1 h with primary antibodies and 45 min with secondary or directly labeled antibodies, all of them dissolved in 0.5% PBS-BSA. Fluorescent images were collected on a Zeiss LSM510/Meta confocal laser-scanning microscope equipped with a 63× oil-immersion objective (numerical aperture [NA] 1.40) and Zeiss/Zen 2011 software.

Live HUVEC FRET measurements

Glass coverslips, containing transfected HUVECs, were placed in an Attofluor cell chamber (Thermo Scientific) 16–20 h after electroporation. Cells were stimulated as indicated, and live-cell FRET images were collected on a widefield Zeiss Observer Z1 microscope equipped with a 40× oil-immersion objective (NA 1.3), an HXP 120-V excitation light source, and Zeiss/Zen 2011 software. CFP was excited using a FRET filter cube with Exciter ET 436/20 and a 455 dichroic longpass (DCLP) mirror (Chroma, Bellows Falls, VT). Emission light was directed to a second dichroic mirror (510 DSCP; Chroma, Bellows Falls, VT) and simultaneously captured with two individual Hamamatsu ORCA-R2 digital charge-coupled device cameras. CFP emission (455–510) was captured on the first camera via an ET 480/40-nm emission filter (Chroma, Bellows Falls, VT). Emission wavelengths of >510 (YFP) were captured on the second camera by using an ET 540/40-nm emission filter (Ludl Electronics Products, Hawthorne, NY). FRET image and ratio analysis was performed in ImageJ according to Timmerman *et al*. (2015) and Reinhard *et al*. (2016).

Static HeLa cell FRET measurements

HeLa cells were transfected as indicated, and glass coverslips were placed in Attofluor cell chambers 16–20 h after transfection. Live-cell FRET images were collected on a widefield Axiovert 200M microscope (Carl Zeiss GmbH) equipped with a Plan-Neofluor 40× oil-immersion objective (NA 1.3), a xenon arc lamp with monochromator (Cairn Research, Faversham, Kent, UK), and Metamorph 6.1 software. Images were acquired using a cooled charged-coupled device camera (Coolsnap HQ, Roper Scientific, Tucson, AZ). CFP was excited at 420 nm (slit width, 30 nm) via a 455 DCLP dichroic mirror, and emission light was directed to a 470/30-nm emission filter. Using a rotating emission filter wheel, YFP emission was directed to a 535/30-nm emission filter. Red fluorescent protein was excited at 570 nm (slit width, 10 nm) via a 585 DCXR dichroic mirror, and in turn emission light was directed to a 620/60-nm emission filter. All image acquisitions were background corrected, and YFP/CFP FRET ratios were bleed-through corrected (55%) for the CFP leakage into the YFP channel.

Live HUVEC morphology change measurements

Transfected HUVECs on glass coverslips were placed in Attofluor cell chambers 16–20 h after transfection. Image collection was performed on the microscope systems as described above. Image analysis was performed in ImageJ; after background subtraction, a smooth filter was used to reduce the noise. Next, a threshold was applied, creating binary images with values of either 255 (signal) or 0 (no signal). Binary images of the prestimulated and stimulated condition were then subtracted by 254 and 253, respectively. These two images were summed, creating image values of 0 (representing the background, displayed in black), 1 (representing contraction, displayed in red), 2 (representing expansion, displayed in blue), and 3 (representing unchanged areas, displayed in white).

ACKNOWLEDGMENTS

The cDNA-encoding p115 was a kind gift of P. Sternweis (UT Southwestern Medical Center). M.M. was supported by Chemische Wetenschappen–Excellent CHemisch Onderzoek (CW-ECHO) Grant no. 711.013.009, and Y.W. was supported by the National Institutes of Health (GM117061).

REFERENCES

Aird WC (2007a). Phenotypic heterogeneity of the endothelium: I. Structure, function, and mechanisms. Circ Res 100, 158–173.

Aird WC (2007b). Phenotypic heterogeneity of the endothelium: II. Representative vascular beds. Circ Res 100, 174–190.

Ancellin N, Colmont C, Su J, Li Q, Mittereder N, Chae S-S, Stefansson S, Liau G, Hla T (2002). Extracellular export of sphingosine kinase-1 enzyme. Sphingosine 1-phosphate generation and the induction of angiogenic vascular maturation. J Biol Chem 277, 6667–6675.

Barr AJ, Brass LF, Manning DR (1997). Reconstitution of receptors and GTP-binding regulatory proteins (G proteins) in Sf9 cells. A direct evaluation of selectivity in receptor.G protein coupling. J Biol Chem 272, 2223–2229.

Berdyshev EV, Gorshkova IA, Garcia JG N, Natarajan V, Hubbard WC (2005). Quantitative analysis of sphingoid base-1-phosphates as bisacetylated derivatives by liquid chromatography-tandem mass spectrometry. Anal Biochem 339, 129–136.

Breslin JW, Zhang XE, Worthylake RA, Souza-Smith FM (2015). Involvement of local lamellipodia in endothelial barrier function. PLoS One 10, e0117970.

Burridge K, Doughman R (2006). Front and back by Rho and Rac. Nat Cell Biol 8, 781–782.

Caligan TB, Peters K, Ou J, Wang E, Saba J, Merrill AH (2000). A high-performance liquid chromatographic method to measure sphingosine 1-phosphate and related compounds from sphingosine kinase assays and other biological samples. Anal Biochem 281, 36–44.

Dejana E (1996). Endothelial adherens junctions: implications in the control of vascular permeability and angiogenesis. J Clin Invest 98, 1949–1953.

Dejana E, Orsenigo F, Lampugnani MG (2008). The role of adherens junctions and VE-cadherin in the control of vascular permeability. J Cell Sci 121, 2115–2122.

Fernández-Pisonero I, Dueñas AI, Barreiro O, Montero O, Sánchez-Madrid F, García-Rodríguez C (2012). Lipopolysaccharide and sphingosine-1-phosphate cooperate to induce inflammatory molecules and leukocyte adhesion in endothelial cells. J Immunol 189, 5402–5410.

Galvani S, Sanson M, Blaho VA, Swendeman SL, Obinata H, Conger H, Dahlbäck B, Kono M, Proia RL, Smith JD, Hla T (2015). HDL-bound sphingosine 1-phosphate acts as a biased agonist for the endothelial cell receptor S1P1 to limit vascular inflammation. Sci Signal 8, ra79.

Garcia JG, Liu F, Verin AD, Birukova A, Dechert MA, Gerthoffer WT, Bamberg JR, English D (2001). Sphingosine 1-phosphate promotes endothelial cell barrier integrity by Edg-dependent cytoskeletal rearrangement. J Clin Invest 108, 689–701.

Giannotta M, Trani M, Dejana E (2013). VE-cadherin and endothelial adherens junctions: active guardians of vascular integrity. Dev Cell 26, 441–454.

Goedhart J, van Weeren L, Adjobo-Hermans MJW, Elzenaar I, Hink MA, Gadella TWJ (2011). Quantitative co-expression of proteins at the single cell level – application to a multimeric FRET sensor. PLoS One 6, e27321.

Guan Z, Singletary ST, Cook AK, Hobbs JL, Pollock JS, Inscho EW (2014). Sphingosine-1-phosphate evokes unique segment-specific vasoconstriction of the renal microvasculature. J Am Soc Nephrol 25, 1774–1785.

Hänel P, Andréani P, Gräler MH (2007). Erythrocytes store and release sphingosine 1-phosphate in blood. FASEB J 21, 1202–1209.

Hart MJ, Jiang X, Kozasa T, Roscoe W, Singer WD, Gilman AG, Sternweis PC, Bollag G (1998). Direct stimulation of the guanine nucleotide exchange activity of p115 RhoGEF by Galpha13. Science 280, 2112–2114.

van Hinsbergh VWM, Eringa EC, Daemen MJAP ((2015). Neovascularization of the atherosclerotic plaque: interplay between atherosclerotic lesion, adventitia-derived microvessels and perivascular fat. Curr Opin Lipidol 26, 405–411.

Inoue T, Heo WD, Grimley JS, Wandless TJ, Meyer T (2005). An inducible translocation strategy to rapidly activate and inhibit small GTPase signaling pathways. Nat Methods 2, 415–418.

Ito K, Anada Y, Tani M, Ikeda M, Sano T, Kihara A, Igarashi Y (2007). Lack of sphingosine 1-phosphate-degrading enzymes in erythrocytes. Biochem Biophys Res Commun 357, 212–217.

Jaffe AB, Hall A (2005). Rho GTPases: biochemistry and biology. Annu Rev Cell Dev Biol 21, 247–269.

Kedziora KM, Leyton-Puig D, Argenzio E, Boumeester AJ, van Butselaar B, Yin T, Wu YI, van Leeuwen FN, Innocenti M, Jalink K, Moolenaar WH (2016). Rapid remodeling of invadosomes by G_i-coupled receptors. J Biol Chem 291, 4323–4333.

Kobayashi N, Nishi T, Hirata T, Kihara A, Sano T, Igarashi Y, Yamaguchi A (2006). Sphingosine 1-phosphate is released from the cytosol of rat platelets in a carrier-mediated manner. J Lipid Res 47, 614–621.

Korn C, Augustin HG (2015). Mechanisms of vessel pruning and regression. Dev Cell 34, 5–17.

Lampugnani MG ((1995). The molecular organization of endothelial cell to cell junctions: differential association of plakoglobin, beta-catenin, and alpha- catenin with vascular endothelial cadherin (VE-cadherin). J Cell Biol 129, 203–217.

Lee MJ, Thangada S, Claffey KP, Ancellin N, Liu CH, Kluk M, Volpi M, Sha'afi RI, Hla T (1999). Vascular endothelial cell adherens junction assembly and morphogenesis induced by sphingosine-1-phosphate. Cell 99, 301–312.

Lin B, Yin T, Wu YI, Inoue T, Levchenko A (2015). Interplay between chemotaxis and contact inhibition of locomotion determines exploratory cell migration. Nat Commun 6, 6619.

Liu F, Verin AD, Wang P, Day R, Wersto RP, Chrest FJ, English DK, Garcia JGN (2001). Differential regulation of sphingosine-1-phosphate- and VEGF-induced endothelial cell chemotaxis. Am J Respir Cell Mol Biol 24, 711–719.

Mahajan-Thakur S, Böhm A, Jedlitschky G, Schrör K, Rauch BH (2015). Sphingosine-1-phosphate and its receptors: A mutual link between blood coagulation and inflammation. Mediators Inflamm 2015, 831059.

Marinissen MJ, Servitja J-M, Offermanns S, Simon MI, Gutkind JS (2003). Thrombin protease-activated receptor-1 signals through Gq- and G13-initiated MAPK cascades regulating c-Jun expression to induce cell transformation. J Biol Chem 278, 46814–46825.

Mehta D, Malik AB (2006). Signaling mechanisms regulating endothelial permeability. Physiol Rev 86, 279–367.

Nourshargh S, Hordijk PL, Sixt M (2010). Breaching multiple barriers: leukocyte motility through venular walls and the interstitium. Nat Rev Mol Cell Biol 11, 366–378.

Obinata H, Gutkind S, Stitham J, Okuno T, Yokomizo T, Hwa J, Hla T (2014). Individual variation of human $S1P_1$ coding sequence leads to heterogeneity in receptor function and drug interactions. J Lipid Res 55, 2665–2675.

Offermanns S, Laugwitz KL, Spicher K, Schultz G (1994). G proteins of the G12 family are activated via thromboxane A2 and thrombin receptors in human platelets. Proc Natl Acad Sci USA 91, 504–508.

Panetti TS (2002). Tyrosine phosphorylation of paxillin, FAK, and p130CAS: effects on cell spreading and migration. Front Biosci 7, d143–d150.

Pappenheimer JR, Renkin EM, Borrero LM (1951). Filtration, diffusion and molecular sieving through peripheral capillary membranes; a contribution to the pore theory of capillary permeability. Am J Physiol 167, 13–46.

Poti F, Simoni M, Nofer J-R (2014). Atheroprotective role of high-density lipoprotein (HDL)-associated sphingosine-1-phosphate (S1P). Cardiovasc Res 103, 395–404.

Putyrski M, Schultz C (2011). Switching heterotrimeric G protein subunits with a chemical dimerizer. Chem Biol 18, 1126–1133.

Pyne NJ, Pyne S (2010). Sphingosine 1-phosphate and cancer. Nat Rev Cancer 10, 489–503.

Reinhard NR, van Helden SF, Anthony EC, Yin T, Wu YI, Goedhart J, Gadella TWJ, Hordijk PL (2016). Spatiotemporal analysis of RhoA/B/C activation in primary human endothelial cells. Sci Rep 6, 25502.

Ridley AJ (2006). Rho GTPases and actin dynamics in membrane protrusions and vesicle trafficking. Trends Cell Biol 16, 522–529.

Ridley AJ (2015). Rho GTPase signalling in cell migration. Curr Opin Cell Biol 36, 103–112.

Sanchez T, Skoura A, Wu MT, Casserly B, Harrington EO, Hla T (2007). Induction of vascular permeability by the Sphingosine-1-Phosphate Receptor-2 (S1P2R) and its downstream effectors ROCK and PTEN. Arterioscler Thromb Vasc Biol 27, 1312–1318.

Sander EE, ten Klooster JP, van Delft S, van der Kammen RA, Collard JG (1999). Rac downregulates Rho activity: reciprocal balance between both GTPases determines cellular morphology and migratory behavior. J Cell Biol 147, 1009–1022.

Schaefer A, Hordijk PL (2015). Cell-stiffness-induced mechanosignaling - a key driver of leukocyte transendothelial migration. J Cell Sci 128, 2221–2230.

Schaller MD, Parsons JT (1995). pp125FAK-dependent tyrosine phosphorylation of paxillin creates a high-affinity binding site for Crk. Mol Cell Biol 15, 2635–2645.

Siflinger-Birnboim A, del Vecchio PJ, Cooper JA, Blumenstock FA, Shepard JM, Malik AB (1987). Molecular sieving characteristics of the cultured endothelial monolayer. J Cell Physiol 132, 111–117.

Sternweis PC, Carter AM, Chen Z, Danesh SM, Hsiung Y, Singer WD (2007). Regulation of Rho guanine nucleotide exchange factors by G proteins. Adv Protein Chem 74, 189–228.

Timmerman I, Heemskerk N, Kroon J, Schaefer A, van Rijssel J, Hoogenboezem M, van Unen J, Goedhart J, Gadella TW Jr, Yin T, *et al.* (2015). A local VE-cadherin and Trio-based signaling complex stabilizes endothelial junctions through Rac1. J Cell Sci 128, 3041–3054.

van Unen J, Reinhard NR, Yin T, Wu YI, Postma M, Gadella TWJ, Goedhart J (2015). Plasma membrane restricted RhoGEF activity is sufficient for RhoA-mediated actin polymerization. Sci Rep 5, 14693.

van Unen J, Stumpf AD, Schmid B, Reinhard NR, Hordijk PL, Hoffmann C, Gadella TWJ, Goedhart J (2016). A new generation of FRET sensors for robust measurement of Gαi1, Gαi2 and Gαi3 activation kinetics in single cells. PLoS One 11, e0146789.

Del Vecchio PJ, Siflinger-Birnboim A, Shepard JM, Bizios R, Cooper JA, Malik AB (1987). Endothelial monolayer permeability to macromolecules. Fed Proc 46, 2511–2515.

Vouret-Craviari V, Bourcier C, Boulter E, van Obberghen-Schilling E (2002). Distinct signals via Rho GTPases and Src drive shape changes by thrombin and sphingosine-1-phosphate in endothelial cells. J Cell Sci 115, 2475–2484.

Welch CM, Elliott H, Danuser G, Hahn KM (2011). Imaging the coordination of multiple signalling activities in living cells. Nat Rev Mol Cell Biol 12, 749–756.

Wettschureck N, Offermanns S (2005). Mammalian G proteins and their cell type specific functions. Physiol Rev 85, 1159–1204.

Wilkerson BA, Grass GD, Wing SB, Argraves WS, Argraves KM (2012). Sphingosine 1-phosphate (S1P) carrier-dependent regulation of endothelial barrier: high density lipoprotein (HDL)-S1P prolongs endothelial barrier enhancement as compared with albumin-S1P via effects on levels, trafficking, and signaling of S1P1. J Biol Chem 287, 44645–44653.

Xiong Y, Hla T (2014). S1P control of endothelial integrity. In: Current Topics in Microbiology and Immunology, 378, ed. MBA Oldstone and H Rosen, Springer International Publishing, 85–105.

Yang L, Yatomi Y, Miura Y, Satoh K, Ozaki Y (1999). Metabolism and functional effects of sphingolipids in blood cells. Br J Haematol 107, 282–293.

Yatomi Y, Igarashi Y, Yang L, Hisano N, Qi R, Asazuma N, Satoh K, Ozaki Y, Kume S (1997a). Sphingosine 1-phosphate, a bioactive sphingolipid abundantly stored in platelets, is a normal constituent of human plasma and serum. J Biochem 121, 969–973.

Yatomi Y, Welch RJ, Igarashi Y (1997b). Distribution of sphingosine 1-phosphate, a bioactive sphingolipid, in rat tissues. FEBS Lett 404, 173–174.

Zhang G, Yang L, Kim GS, Ryan K, Lu S, O'Donnell RK, Spokes K, Shapiro N, Aird WC, Kluk MJ, *et al.* (2013). Critical role of sphingosine-1-phosphate receptor 2 (S1PR2) in acute vascular inflammation. Blood 122, 443–455.